Computational metallurgy and changes of scale / Métallurgie numérique et changements d'échelle

Microstructures and rheology of the Earth's upper mantle inferred from a multiscale approach

Microstructures et rhéologie du manteau terrestre supérieur déduites d'une approche multi-échelle

Olivier Castelnau [a,*], Patrick Cordier [b], R.A. Lebensohn [c], Sébastien Merkel [b], Paul Raterron [b]

[a] *PIMM, CNRS, arts et métiers ParisTech, 151, boulevard de l'Hopital, 75013 Paris, France*
[b] *Unité matériaux et transformations, bâtiment C6, université Lille 1, 59655 Villeneuve d'Ascq, France*
[c] *MST8 - MS G755, Los Alamos National Laboratory, Los Alamos, NM 87545, USA*

Keywords:
Olivine
Dislocations
High pressure
Viscoplasticity
Polycrystal
Homogenization
Earth mantle

Mots-clés :
Olivine
Dislocations
Haute pression
Viscoplasticité
Polycristal
Homogénéisation
Manteau terrestre

A B S T R A C T

The strongly anisotropic rheology of olivine polycrystals, associated to their microstructure, constitutes a key feature affecting the dynamics of the Earth's upper mantle. High pressure deformation experiments carried out on olivine single crystals under synchrotron radiation, together with estimations of lattice friction based on first-principle calculations, show a transition from easy [100] to easy [001] slips as pressure and temperature (thus depth) increases. We input these data at the slip system level into the second-order extension of the self-consistent scheme to assess microstructure evolution along a typical flow pattern beneath an oceanic spreading center.

R É S U M É

La forte anisotropie rhéologique des polycristaux d'olivine, associée à leur microstructure, est un aspect majeur affectant la dynamique du manteau terrestre supérieur. Des expériences de déformation sous haute pression et en rayonnement synchrotron de monocristaux d'olivine, complétées par des calculs ab initio de friction de réseau, montrent une transition du système « mou » depuis [100] vers [001] quand la pression et la température (et donc la profondeur in situ) augmentent. Nous avons introduit ces données à l'échelle du système de glissement dans l'extension du second-ordre du schéma auto-cohérent afin d'appréhender les évolutions de microstructure le long d'un écoulement typique sous une dorsale océanique.

1. Introduction

Large scale processes in the Earth, such as mantle convection, earthquakes, and plate tectonics, involve plastic deformation of rocks. As such, rheology and microstructures are key parameters affecting dynamical processes in the mantle [1,2],

* Corresponding author.
E-mail addresses: olivier.castelnau@paris.ensam.fr (O. Castelnau), Patrick.Cordier@univ-lille1.fr (P. Cordier), lebenso@lanl.gov (R.A. Lebensohn), sebastien.merkel@univ-lille1.fr (S. Merkel), Paul.Raterron@univ-lille1.fr (P. Raterron).

1631-0705/$ – see front matter
doi:10.1016/j.crhy.2010.07.011

which lies between the crust and 2900 km beneath the surface. However, the study of deep Earth rheology raises significant difficulties, including the complexity of the crystallographic structure of minerals, extreme conditions of pressure and temperature, and time and size scaling issues between laboratory results and the Earth's mantle.

In the last few years, tremendous progress has been made with the development of experimental techniques for the study of rheology at high pressure (see [3] for a review) and the application of first-principle methods for the study of dislocation structure and mobility in deep Earth minerals [4–7]. In parallel, numerical modeling of polycrystal behavior (mean-field homogenization methods) has been carried out to understand the behavior of deep Earth minerals [8,9]. More recently, the theoretical formulation of these methods has been greatly improved [10,11] providing nowadays very accurate results even for highly anisotropic non-linear materials such as minerals [12–14].

Olivine is the most important mineral of the upper mantle (volume fraction of $\sim$60%) and is stable up to a depth of 410 km for which pressure and temperature reach about 13.7 GPa and 1760 K. It is a silicate with the general composition $(Mg, Fe)_2SiO_4$ and it crystallizes in the orthorhombic system (space group *Pbnm*). Recently, deformation data obtained at high pressure have shown a transition from dominant slip of dislocations exhibiting a [100] Burgers vector at pressures below $\sim$3 GPa to dominant [001] slip at higher pressures [15–19]. This has also been supported by numerical modeling which shows that the relative strength of the [100](010) slip system increases significantly with pressure, when compared to [001](010) [4,5]. These new findings raised debates in the literature, e.g. [20–22], and have important implications for the understanding of dynamic processes at depth greater that 200 km.

In this work, we propose a multiscale numerical modeling to investigate the influence of this [100] to [001] slip transition on crystallographic textures and associated viscoplastic anisotropy in the mantle. The first section (Section 2) of the paper describes experimental and numerical methods used to study plastic deformation of olivine under extreme conditions of pressure and temperature, at different scales (from the scale of the crystal defect to the polycrystal scale). Section 3 is devoted to the description of homogenization methods used to bridge single-crystal and polycrystal behaviors. One originality of our approach relies on the use in the micromechanical model of the pressure dependent slip system strength as determined in Section 2. Finally, we show an application of this multiscale model to a typical mantle convection pattern.

2. Relative strength of olivine dislocation slip systems

2.1. Insights from single-crystal deformation experiments

The strength of given dislocation slip systems can be quantified by carrying out deformation experiments on single crystals in specific orientations. The crystallographic orientations are chosen to maximize the Resolved Shear Stress (RSS) for a given slip system while minimizing the other slip systems RSS. Best results are obtained when the RSS vanishes for all slip systems but one, a configuration which is achieved in axial compression for two crystal orientations in olivine. Compressing crystals along the so-called $[110]_c$ direction – which forms a 45° angle with both [100] and [010] crystallographic directions, as would the [110] direction in a cubic crystal (hence the *c* index) – only promotes [100] slip in (010) plane, i.e. the RSS in (010) plane along the [100] direction is then half the differential stress $\sigma = \sigma_1 - \sigma_3$, where σ_1 is the principal stress direction. The [001] direction is then perpendicular to σ_1 direction, which prevents glide of [001] dislocations as well as [100] glide in (001) plane (RSS = 0). Conversely, compressing crystals along the $[011]_c$ direction (at 45° from both [010] and [001]) only promotes the [001](010) slip system. San Carlos olivine crystals in both these orientations have been deformed successfully at high temperature T in water poor conditions. These experiments have been carried out at room pressure [23] using a dead load apparatus, and at high pressure up to $P = 8.5$ GPa [19] using a deformation multi-anvil apparatus (D-DIA) coupled with X-ray synchrotron radiation [3,24]. Results from these experiments led to the quantification of [100](010) and [001](010) slip systems' activities at given P, T, and stress conditions [19].

High-temperature dislocation creep in natural Fe-bearing olivine is usually quantified using a phenomenological power creep law, or a combination of power laws, of the form:

$$\dot{\varepsilon} = A\sigma^n f_{O_2}^m \exp\left(-\frac{E^* + PV^*}{RT}\right) \tag{1}$$

where $\dot{\varepsilon}$ is the strain-rate, $\sigma = \sigma_1 - \sigma_3$ the differential stress, n the stress sensitivity, f_{O_2} the oxygen fugacity, E^* and V^* the activation energy and activation volume respectively, A and m other rheological constants, and R the gas constant. The rheological parameters for San Carlos olivine single crystals deformed in axial compression along $[110]_c$ and $[011]_c$ directions are reported in Table 1. Also reported in Table 1 are the rheological parameters for olivine crystals deformed along the $[101]_c$ direction, as measured at room pressure [23] and at high pressure. This third orientation prevents dislocation glide in (010) and maximizes the RSS on both [100](001) and [001](100) potential slip systems. It is not possible at this stage to infer the respective contribution of these slip systems to the overall deformation. Further considerations from numerical modeling will be introduced in Section 2.2 to clarify this issue.

2.2. Insights from first-principle calculations

Micromechanical models as presented in Section 3 require the knowledge of a reference shear stress, often denoted Critical Resolved Shear Stress (CRSS), that expresses the strength of the considered slip system, see Eq. (2) below. The CRSS aims

Table 1
Rheological parameters for San Carlos olivine crystals. A, n, m and E^* from [23]; V^* from [19] for compression directions $[110]_c$ and $[011]_c$, and from Raterron (unpublished data) for $[101]_c$. Because dislocation motions at high temperature involve several basic mechanisms (glide, climb, cross slip, etc.) occurring either sequentially or in parallel, the empirical rheological laws reported in this table have been expressed as combinations of 2 or 3 rheological laws of the form of Eq. (1) whose respective parameters are listed (see [23] for details).

Tableau 1
Paramètres rhéologiques de cristaux d'olivine de San Carlos. A, n, m et E^* d'après [23] ; V^* d'après [19] pour les directions de compression $[110]_c$ et $[011]_c$, et d'après Raterron (données non publiées) pour $[101]_c$. Puisque le mouvement des dislocations à haute température implique plusieurs mécanismes (glissement, montée, glissement dévié, etc.) activés simultanément ou successivement, les lois rhéologiques empiriques indiquées dans ce tableau sont exprimées sous forme d'une combinaison linéaire de 2 ou 3 lois rhéologiques de la forme de l'équation (1) dont les paramètres respectifs sont donnés (voir [23] pour les détails).

Strain-rate [s^{-1}]	A [$MPa^{-n}\,atm^{-m}$]	n	m	E^* [kJ/mol]	V^* [cm^3/mol]
Compression direction $[110]_c \rightarrow [100](010)$ slip system activated $\dot{\varepsilon} = \dot{\varepsilon}_1 + (1/\dot{\varepsilon}_2 + 1/\dot{\varepsilon}_3)^{-1}$					
$\dot{\varepsilon}_1$	0.02	3.5	0.36	230	12
$\dot{\varepsilon}_2$	1.3×10^{22}	3.5	0.10	1000	12
$\dot{\varepsilon}_3$	1.2	3.5	0.15	290	12
Compression direction $[011]_c \rightarrow [001](010)$ slip system activated $\dot{\varepsilon} = \dot{\varepsilon}_1 + \dot{\varepsilon}_2$					
$\dot{\varepsilon}_1$	2.1×10^4	3.5	0.02	540	3
$\dot{\varepsilon}_2$	1.3×10^{22}	3.5	0.10	1000	3
Compression direction $[101]_c \rightarrow [001](100)$ & $[100](001)$ slip systems activated $\dot{\varepsilon} = (1/\dot{\varepsilon}_1 + 1/\dot{\varepsilon}_2)^{-1}$					
$\dot{\varepsilon}_1$	0.65	3.5	0.33	250	12
$\dot{\varepsilon}_2$	5.3×10^{11}	3.5	0.06	690	12

to describe the collective behavior of the dislocations of a given slip system which propagate into the crystal (which might contain other dislocations usually referred to as "forest" dislocations). Dislocation mobility is limited by several interactions with the lattice, with other dislocations, etc. In mantle minerals, it can be anticipated that intrinsic lattice friction is a major factor limiting dislocation mobility. This fact, commonly observed in oxides and ceramics, is even more important in the context of mantle rheology since pressure brings atoms closer, and increases elastic stiffness and consequently lattice friction. The difficulty is that lattice friction is not only constrained by elastic considerations. The fine structure of dislocation cores (at the atomic scale) has profound implications on dislocation mobility (as a rule of thumb, dislocation-core spreading usually enhances mobility).

Numerical modelling of dislocation cores in minerals has only been addressed quite recently. The most straightforward approach consists in calculating an atomistic model of the dislocation core. However, for materials with complex crystal chemistry, these calculations remain at the frontier of present-day computational possibilities when first-principle calculations are considered. The use of empirical potentials, whenever available, has opened the way to such calculations [25–28] but it is then difficult to relate the dislocation-core structures to their mobility. Alternatively, the atomic scale structure and properties of the dislocation core can be inferred from a simplified description of a dislocation such as the one first introduced by Peierls [29] and Nabarro [30]. Originally, the Peierls–Nabarro problem could only be solved in extremely simplified cases, when the inelastic restoring forces in the dislocation core are sinusoidal. Later, Vítek [31] and Christian and Vítek [32] demonstrated that restoring forces are the negative of the derivative of the stacking fault energy with respect to displacement of the two atomic planes across the glide plane. Fortunately, this so-called "generalized stacking fault" or "γ-surface" energy can be calculated at relatively low numerical cost using either empirical potentials or first-principle calculations. It is an efficient way to assess the influence of pressure on lattice friction. After further introduction of the atomic scale description, this approach can even lead to assessment of the lattice friction in the form of the so-called Peierls stress. The Peierls stress, often described as the stress necessary to move a straight dislocation line without thermal activation, is in fact a mechanical assessment of the energy barrier opposed to dislocation motion.

One of the first applications of this model to minerals has been done on olivine. Durinck et al. [4] have shown that γ-surfaces represent a very powerful approach to capture the essence of lattice friction in forsterite (i.e. Fe-free olivine) and the influence that confining pressure has on it. In a further study, γ-surfaces were used to model dislocation-core structures and mobilities in forsterite [5]. These calculations were based on a 1-D resolution of the Peierls–Nabarro equation which can only describe planar core structures spread along the Burgers vector direction. Carrez et al. [7] have compared some of these calculations with fully atomistic calculations based on the cluster model [27]. They show that in some cases, screw dislocations can exhibit complicated 3-D core structures that are not described by a 1-D Peierls–Nabarro model. Further calculations based on the Peierls–Nabarro–Galerkin method have been performed in [33,34]. They show that the (010) plane plays a very special role in the plasticity of olivine. It is only in this plane that dislocations (either [100] or [001]) exhibit a fully planar core. In any other plane, the strong tendency to spread shear in the (010) plane results in non-planar components on screw dislocations and hence on a higher strength. In particular, it is shown that non-planar components on screw dislocations increase the strength of [100](001) and [001](100) at a comparable level. This further implies that experiments performed on $[101]_c$ samples provide information on the CRSS of both slip systems. The [100]{0*kl*}

Table 2
CRSS of olivine slip systems as estimated along a 20 Ma geotherm. Values are normalized with respect to the CRSS of [100](010) that serves as a reference.

Tableau 2
CRSS des systèmes de glissement de l'olivine estimées le long d'un géotherme de 20 Ma. Les valeurs sont normalisées par la CRSS de [100](010) qui est prise comme référence.

Depth [km]	P [GPa]	T [K]	[100](010)	[001](010)	[001](100)	[100](001)	[100]{021}	[001]{110}
60	2.0	1443.7	1	3.20	1.88	1.88	1.88	5.64
75	2.5	1538.3	1	2.08	1.09	1.09	1.09	3.27
90	3.0	1582.0	1	1.95	1.05	1.05	1.05	3.15
105	3.5	1596.2	1	1.86	1.09	1.09	1.09	3.27
120	4.0	1604.2	1	1.73	1.20	1.20	1.20	3.60
135	4.5	1612.2	1	1.60	1.13	1.13	1.13	3.39
150	5.0	1620.3	1	1.50	1.15	1.15	1.15	3.45
165	5.5	1628.3	1	1.40	1.17	1.17	1.17	3.51
180	6.0	1636.3	1	1.32	1.22	1.22	1.22	3.66
195	6.5	1644.3	1	1.22	1.24	1.24	1.24	3.72
210	7.0	1652.4	1	1.13	1.26	1.26	1.26	3.78
225	7.5	1660.4	1	1.04	1.28	1.28	1.28	3.84
240	8.0	1668.4	1	0.96	1.30	1.30	1.30	3.90
255	8.5	1676.4	1	0.88	1.32	1.32	1.32	3.96
270	9.0	1684.5	1	0.81	1.32	1.32	1.32	3.96
285	9.5	1692.5	1	0.74	1.34	1.34	1.34	4.02
300	10.0	1700.5	1	0.67	1.34	1.34	1.34	4.02
315	10.5	1708.5	1	0.61	1.36	1.36	1.36	4.08
330	11.0	1716.6	1	0.55	1.36	1.36	1.36	4.08
345	11.5	1724.6	1	0.51	1.36	1.36	1.36	4.08
360	12.0	1732.6	1	0.46	1.36	1.36	1.36	4.08
375	12.5	1740.6	1	0.42	1.36	1.36	1.36	4.08
390	13.0	1748.7	1	0.38	1.37	1.37	1.37	4.11
405	13.5	1756.7	1	0.35	1.37	1.37	1.37	4.11

and [001]{hk0} slip systems have not been calculated, however, it is assumed that screw dislocations tend here as well to develop out-of-plane components which decrease their mobilities.

2.3. Relative strength of slip systems along a 20 Ma oceanic geotherm

The P and T dependent rheological law (1) can be specialized at the slip system level

$$\dot{\gamma}^{(k)} = \dot{\gamma}_0 \left| \frac{\tau^{(k)}}{\tau_0^{(k)}} \right|^{n^{(k)}-1} \frac{\tau^{(k)}}{\tau_0^{(k)}} \tag{2}$$

with the slip-rate $\dot{\gamma}^{(k)}$ on system (k), a reference slip-rate $\dot{\gamma}_0$, and the CRSS $\tau_0^{(k)}$ of system (k). Such an expression is required for polycrystal modelling based on micromechanical approaches, as presented in the next section. To model olivine aggregate deformation within the Earth's mantle, one thus need to quantify the relative CRSS under in situ conditions. For the [100](010) and [001](010) slip systems, one can use the rheological laws (1) with values reported in Table 1. The Earth's mantle P–T profile with depth, the so-called *geotherm*, has been estimated from geophysical observations in different geological context (continental or oceanic) and is fairly well known. In the following we assume a classical 20 Ma oceanic geotherm (Table 2) which is representative of a young oceanic upper mantle. Differential stress has been estimated in the mantle in the order of 1 MPa, while the oxygen fugacity is set by the iron–wustite and the fayalite–quartz–magnetite equilibria. At room pressure this roughly corresponds to f_{O_2} ranging from 10^{-10} to 10^{-6} atm. We thus assume the average value of $f_{O_2} = 10^{-8}$ atm in the following. Using strain-rates for crystals in $[110]_c$ orientation allows the estimation of a reference strain-rate corresponding to the activation of [100](010) slip system. Similarly, crystal orientations $[011]_c$ and $[101]_c$ are used to infer the rheology of [001](010), [100](001), and [001](100). As for the CRSS estimation of the other systems, namely [100]{021} and [001]{110}, use has to be made of additional considerations from first-principle calculations, as presented above.

Our model for the CRSS of olivine slip systems as a function of depth is presented in Table 2. In this table, CRSS estimates are relative to that of [100](010) which was arbitrarily set to 1 MPa. The CRSS of [100](010) is found to be the smallest at low pressures, indicating that this system could dominate olivine deformation at shallow depth. Yet, [001](010) relative CRSS decreases significantly with increasing pressure and this system becomes the softest at depth greater that ∼240 km. This indicates that [001] slip might be the dominant deformation mechanism at larger depth. The CRSS of [100] dislocations on (001) and {021} planes is found to be similar to that of [001](001). Finally, for system [001]{110}, considerations on dislocation structures would also indicate a CRSS close to that for [001](001). Here however, we were forced to multiply this CRSS by a factor 3 as discussed in Section 3.3.

3. Polycrystal micromechanical modelling

The aim of polycrystal micromechanical models is the evaluation of mechanical interactions occurring between deforming grains. For polycrystals exhibiting a very large viscoplastic anisotropy at the grain scale, such as olivine, strong heterogeneities of stress and strain-rate build up at the inter- and intra-granular scales upon macroscopic deformation of the polycrystal. These heterogeneities have a tremendous influence on the overall polycrystal rheology, as well as on microstructure evolution at large strain. A challenging feature in olivine plasticity is the lack of independent slip systems at the grain level. Indeed, slip systems given in Table 2 do not allow any axial deformation of grains along [100], [010], and [001] lattice directions, since only [100] and [001] Burgers vectors are present. They leave olivine grains with only three independent slip systems, although five independent systems are required – according to the intuitive and so-called von Mises criterion – to accommodate arbitrary plastic deformations. This point has been an issue for earlier micromechanical studies. For example, the uniform stress bound used in [35] only requires a single slip system within a single grain of the whole polycrystal to allow the polycrystal to deform. The earlier extension of the Self-Consistent (SC) scheme used in [8,9] also predicts a finite flow stress with three independent systems, which is another puzzling result. On the other hand, it has been shown that only four independent systems are sufficient (but necessary) for hexagonal polycrystals [36,37]. However, according to [38], this result is model dependent. A recent systematic study based on full-field modelling [12,39] has shown that, effectively, three independent systems are not sufficient for olivine polycrystals (see also [13]), but four systems are enough.

3.1. Full-field modelling

Micromechanical models are necessary to make the link between deformation mechanisms at the sub-grain (or micrometric) and mantle convection (kilometer) scales. Rapid computation of polycrystal behavior can be achieved only with mean-field homogenization techniques, such as those based on the self-consistent scheme. These models rely on a statistical description of the microstructure (spatial arrangement of grains and crystallographic texture), so that the stress and strain-rate heterogeneities within the polycrystal but also within the different crystallographic orientations can be only partly estimated. As discussed above, many of the earlier mean-field estimates led to inconsistent results such as violation of rigorous bounds for the effective potential [40].

To assess the accuracy of micromechanical models, we first apply a full-field numerical technique. The FFT-based formulation for viscoplastic polycrystals is conceived for periodic microstructures submitted to periodic boundary conditions. It provides an accurate solution of the governing equations (within the unavoidable numerical errors associated with the required spatial discretization and the iterative character of the method), and has, in general, better numerical performance than finite element calculations. It was originally developed [41,42] to compute the elastic and elastoplastic response of composites, and later adapted [43] to deal with the viscoplastic deformation of polycrystals. Briefly, the viscoplastic FFT-based formulation consists in iteratively adjusting a compatible strain-rate field, related with an equilibrated stress field through a constitutive potential, such that the average of local work-rates is minimized. The method is based on the fact that the local mechanical response of a heterogeneous medium can be calculated as a convolution integral between Green functions associated with appropriate fields of a linear reference homogeneous medium and the actual heterogeneity field. For periodic media, use can be made of the Fourier transform to reduce convolution integrals in real space to simple products in Fourier space, leading thus to efficient computations. However, the actual heterogeneity field depends precisely on the a priori unknown mechanical fields. Therefore, an iterative scheme has to be implemented to obtain, upon convergence, a compatible strain-rate field and a stress field in equilibrium.

Application of this full-field method to olivine has been performed using periodic polycrystal microstructures as that shown in Fig. 1a. They are generated by a Voronoi tessellation and comprise 32 grains exhibiting a random crystallographic orientation. As for the single grain behavior, we have used here CRSS values such that slip on [100](010) and [100](001) is promoted, as in [14]. To address the issue of the necessary fourth independent slip system, a physically relevant method would be to consider the climb of edge dislocations as recently proposed in [44]. However, very little is known about the actual contribution of climb to olivine deformation. TEM observation of naturally deformed olivines often show evidences of subgrain boundaries. This can be interpreted as an indication of climb processes although these microstructures might just reflect post-deformation recovery processes. Another possibility to account for the polycrystal deformation with insufficient numbers of slip systems might involve grain boundary processes (grain boundary sliding, grain boundary migration, grain rotation, etc.). These processes involve point defect diffusion and are likely to be, to a first-order, isotropic. Solving this issue is however beyond the scope of the present work. Here, we follow a substitute method similar to that used in many previous works (e.g., see [8,9]). The idea is to introduce an additional deformation mechanism to provide enough degree of freedom to deform the material. For sake of simplicity, this deformation mechanism is introduced in the form of additional slip systems of the $\langle 1\bar{1}0\rangle\{111\}$ type. These slip systems have no physical reality, but they are chosen so as to provide an (almost) isotropic additional deformation mechanism that can be activated locally to relieve stress concentrations arising from insufficient slip systems. The corresponding CRSS is taken large enough (100 times larger than that for [100](010)) so that the contribution of these systems to the overall deformation remains minimal ($\sim$ few percents).

Among the many results that can be inferred for full-field computations, we present in Fig. 1b the link between local (von Mises) equivalent stress and local equivalent strain-rate inside the deforming polycrystal. Obviously, no clear trend is

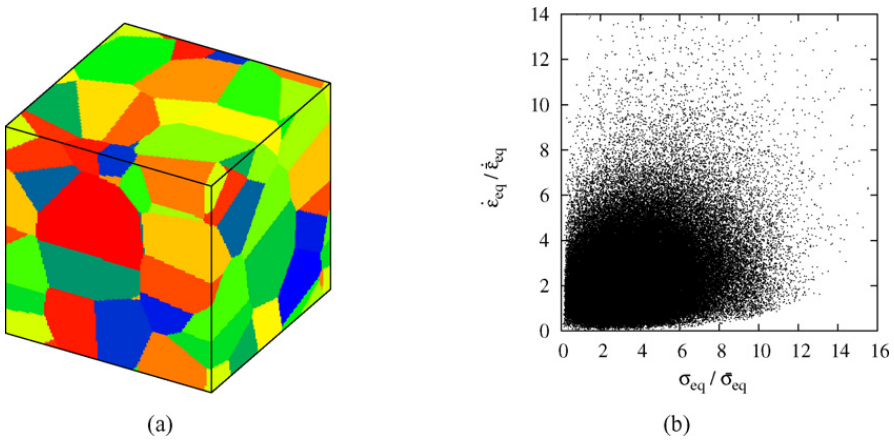

Fig. 1. (a) Typical polycrystal microstructure considered for the FFT full-field model. It is generated by Voronoi tessellation for which spatial periodicity is enforced, and comprises 32 randomly oriented grains. (b) Relation between local $\dot{\varepsilon}_{eq}$ and σ_{eq} (normalized by the respective overall quantities) at each Fourier point of the polycrystal deformed under uniaxial compression. Each grain is represented by 8192 dots on average.

Fig. 1. (a) Microstructure typique d'un polycristal, considérée pour le modèle FFT en champ complet. Elle est générée à partir d'un diagramme de Voronoï périodique, et comprend 32 grains d'orientation aléatoire. (b) Relation entre les quantités locales $\dot{\varepsilon}_{eq}$ et σ_{eq} (normalisées par les valeurs effectives respectives) à chaque point de Fourier dans le polycristal déformé en compression uniaxiale. Chaque grain est représenté par en moyenne 8192 points.

observed, the local equivalent strain-rate can be high (or low) with either a low or high local stress level, depending on the spatial position of the observation point. This feature expresses the tremendous effect of the intergranular interactions: the local mechanical state inside the polycrystal is not only guided by the local crystallographic orientation of the considered grain, but it is also highly influenced by the neighborhood. Therefore, the microstructure cannot be described as consisting of "hard" and "soft" grains depending of their orientation, as sometimes proposed in the literature. Only so-called *phase average* stress and stain-rate (i.e. averages over a large number of grains exhibiting the same crystallographic orientation) are correlated [13]. It should be also emphasized that local equivalent stress and strain-rate are generally much larger than their macroscopic counterpart (Fig. 1b). A material point is thus generally submitted to much more drastic mechanical conditions than the average polycrystal. Obviously, this effect gets less pronounced if isotropic diffusion based processes become the dominant deformation mechanisms (e.g. as temperature increases) compared to dislocation glide.

3.2. Second-order self-consistent estimate

Predictions of polycrystal behavior can be obtained with mean-field homogenization methods at a much reduced numerical effort compared to full-field FFT computations. For *linear behavior* such as elasticity or linear viscosity, the SC model proposed by [45,46] provides results in excellent agreement with full-field FFT results, for both 2-D [47] and 3-D [48] polycrystals. This model relies on a random geometrical grain arrangement exhibiting some specific statistical properties such as an infinite graduation of sizes [49]. It has often been described as if the interaction between each grain and its surrounding could be approximated by the interaction between one ellipsoidal grain with the same lattice orientation as the original grain and a homogeneous equivalent medium whose behavior represents that of the polycrystal, taking thus advantage of the analytical solution of Eshelby [50] for the inclusion/matrix interaction, which results in uniform mechanical fields inside the grain. This latter interpretation of the SC model turns out to be incorrect, since stress and strain-rate heterogeneities within each crystal orientation (so-called intra-phase heterogeneities) do not vanish, see e.g. [51,52].

The extension of the SC theory to *non-linear* viscoplasticity includes several technical difficulties, in particular a linearization of the polycrystal that can critically affect the results and even lead to inconsistencies [53]. A robust linearization method has been proposed only recently, leading to the *second-order self-consistent* (SO) model [10] that has been shown to provide quantitative agreement with several "exact" numerical solutions in different contexts, e.g. for fiber-reinforced composites [11] and various polycrystals [12]. By construction, this model also complies with rigorous upper bounds. It is based on an optimal solution for the related variational problem, leading to the construction of the so-called *N-Phase Linear Comparison Polycrystal* (LCP) from which the behavior of the (actual) non-linear polycrystal of interest can be derived. The accuracy of the SO approach comes from the definition of the LCP which includes information on field heterogeneities. Indeed, it depends on both the phase average stress (first moment of the stress distribution) and phase average variance (second moment). It can be noted that although models based on the SC formulations (and particularly the second-order extension) efficiently condense the very large complexity of the mechanical problem into a small set of compact equations, the geophysical community has been hesitant to move beyond ad hoc formulations such as those proposed by [54–56], with limitations described above.

Fig. 2 provides a comparison of results of the SO model with reference solutions provided by the FFT numerical approach, for the case of olivine with the same CRSS as in Section 3.1. For doing this, ensemble average over 50 randomly generated FFT microstructures has been taken, in order to improve the statistical relevance of results. The effective flow stress at the polycrystal level is given as a function of the CRSS of $\langle 1\bar{1}0\rangle\{111\}$. In Fig. 2a, only three independent systems remain in grains

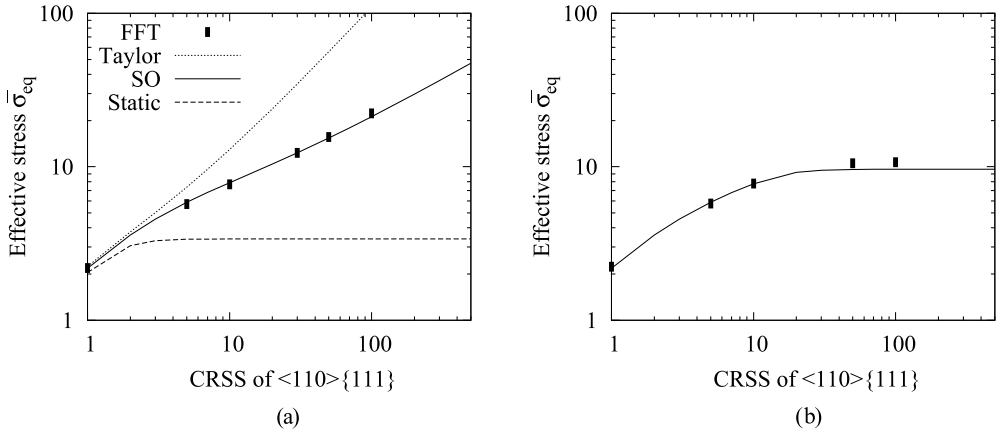

Fig. 2. (a) Evolution of the effective equivalent stress for the polycrystal with the CRSS of the additional systems $\langle 1\bar{1}0\rangle\{111\}$. Results provided by the Reuss and Taylor bounds are provided for comparison. (b) A supplementary system $\langle\bar{1}01\rangle\{101\}$ with a CRSS of 10 is added.

Fig. 2. (a) Evolution de la contrainte effective équivalente du polycristal, en fonction de la CRSS du système additionnel $\langle 1\bar{1}0\rangle\{111\}$. Les résultats des bornes de Reuss et Voigt sont donnés pour comparaison. (b) Un système supplémentaire $\langle\bar{1}01\rangle\{101\}$ avec une CRSS de 10 est ajouté.

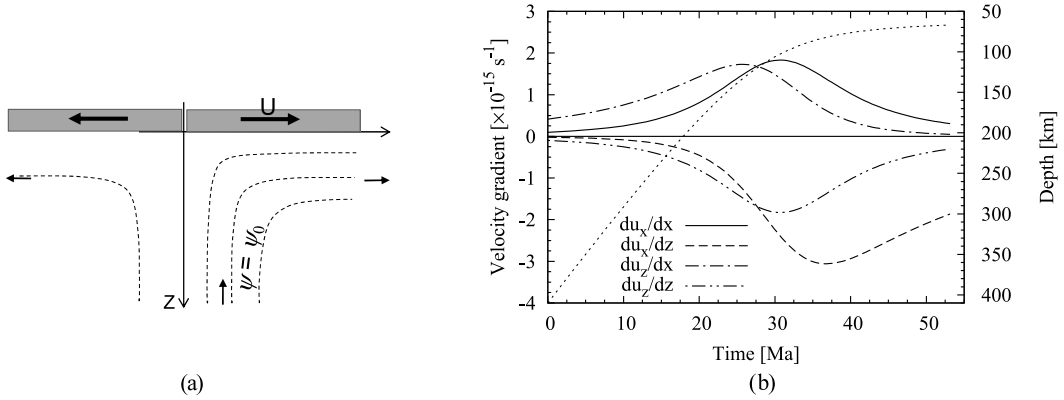

Fig. 3. (a) Typical flow beneath an idealized oceanic ridge. (b) Velocity gradient along the streamline described by (3) for $\psi_0 = 1200$ m^2/a and $U = 2$ cm/a. The thin dash line provides the correspondence between travel time and in situ depth.

Fig. 3. (a) Ecoulement typique sous un ridge océanique. (b) Gradient de vitesse le long de la ligne de courant décrite par (3) pour $\psi_0 = 1200$ m^2/a et $U = 2$ cm/a. Le trait pointillé fin donne la correspondance entre le temps et la profondeur in situ.

as the CRSS of $\langle 1\bar{1}0\rangle\{111\}$ tends to $+\infty$, and consequently the polycrystal becomes infinitely stiff. In Fig. 2b, an additional slip system $\{101\}\langle\bar{1}01\rangle$ is introduced (a way to mimic, although not very accurately, deformation that dislocation climb could produce). Unlike $\langle 1\bar{1}0\rangle\{111\}$, this last system does not allow grains to deform axially along [010] lattice direction. Therefore, grains exhibit now four independent systems as the CRSS of $\langle 1\bar{1}0\rangle\{111\}$ tends to $+\infty$. Note the saturation of the flow stress at large CRSS, showing that these four independent systems are sufficient for olivine polycrystals to deform. In both figures, and for the wide range of CRSS of $\langle 1\bar{1}0\rangle\{111\}$ considered, the agreement between the SO model and the "exact" FFT solution is almost perfect. The huge gap with simpler formulations, such as the Reuss (uniform stress) or Taylor (uniform strain-rate) bounds, is also worth noticing. This shows that too simple or ad hoc formulations should be used only with special care. Present results prove that the SO model handles correctly, qualitatively and quantitatively, the complex mechanical problem of non-linear, strongly anisotropic, and randomly mixed olivine grains interacting with each other. Therefore, this SO formulation is ideally suited to investigate how P–T dependent CRSS may affect rheology and microstructure evolution for condition prevailing in the upper mantle. In the next section, CRSS evolution along a geotherm, as described in Section 2, will be coupled with the SO formulation.

3.3. Microstructure evolution due to convection in the Earth's mantle

In the Earth's upper mantle, Lattice Preferred Orientation (LPO) develops as the result of plastic deformation of mantle minerals associated with large-scale convective flow. For this very first application of the proposed multiscale approach, we consider a simple in situ flow pattern, i.e. an upwelling mantle flow representative for typical oceanic spreading centers (Fig. 3a). The 2-D flow is passively driven by a lithospheric rigid plate moving at a constant speed U along the horizontal direction **x**. The flow is symmetric about the plane (**x**, **z**), with the vertical (downwards) axis **z**. Such a flow admits an analytical solution for the stream function ψ next to the flow corner [57]

$$\psi = -\frac{2U}{\pi} z \arctan\frac{x}{z} \tag{3}$$

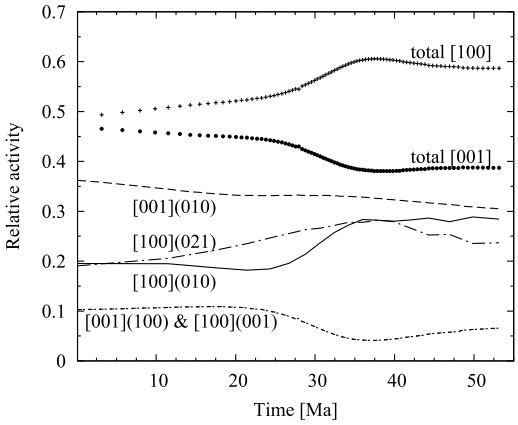

Fig. 4. Predicted activity of slip systems along the streamline. Systems for which the activity is always less than 0.1 are not shown. The total contributions of slip on [100] and [001] are also shown.

Fig. 4. Prédiction de l'activité des systèmes de glissement le long de la ligne d'écoulement. Les systèmes pour lesquels l'activité est inférieure à 0,1 ne sont pas montrés. Les contributions totales de [100] et [001] sont également indiquées.

leading to the velocity gradient plotted in Fig. 3b and the following expressions for the strain-rate components

$$\dot{\varepsilon}_{xx} = \frac{2U}{\pi}\frac{2x^2 z}{(x^2+z^2)^2} = -\dot{\varepsilon}_{zz}, \qquad \dot{\varepsilon}_{xz} = -\frac{2U}{\pi}\frac{x(x^2-z^2)}{(x^2+z^2)^2} \tag{4}$$

Here we consider the case of a typical spreading rate $U = 2$ cm/a, and the streamline corresponding to $\psi = 1200$ m^2/a which ends up at the asymptotic depth $z = 60$ km as $x \to +\infty$. The olivine polycrystal of interest exhibits an isotropic behavior (i.e. a random crystallographic texture) at depth 410 km (corresponding to $x \approx 96$ km), and we will consider its deformation along the streamline up to the position $x = 400$ km (i.e. $z \approx 67$ km). When subjected to the velocity gradient given above, the polycrystal needs about 52 Ma to travel the whole streamline, the flow corner being reached after ∼30 Ma. With a typical strain-rate of $\sim 10^{-15}$ s^{-1}, a total equivalent strain of 2.1 is reached at the end point. The chosen streamline contains several typical aspects for a flow field near a plate boundary, in particular rapid changes of the deformation path as also shown by more realistic convective flow modeling [58]. Flow evolves from nearly vertical simple shear in the upwelling region, to significant axial straining around the flow corner, and ends with a nearly horizontal simple shear far from the spreading center.

To investigate the possible effect that slip system strength may have on in situ microstructures, we use the velocity gradient of Fig. 3b as input for the SO model, together with the P–T dependent CRSS provided in Table 2. Unlike the preceding section, instead of introducing additional arbitrary slip systems such as $\langle 1\bar{1}0\rangle\{111\}$, we follow here a physically more sound approach: we introduce in the model an isotropic and linear viscosity that is likely to represent diffusion processes that might occur in situ. The viscosity of this accommodation mechanism is however not very well constrained by experimental data. Therefore, it is set stiff enough compared to dislocation slip so that its contribution to the deformation of grains remains very small. In these conditions, it has also no effects on texture evolution described below.

Fig. 4 shows the evolution of slip system activities as the polycrystal travels the whole streamline. Here, the activity of a slip system is defined as the total slip-rate (i.e. the sum over all grains) on this system divided by the total slip-rate on all slip systems. It thus provides an estimation of the contribution of a given system to the overall polycrystal deformation. For sake of clarity, the activities of [001]{110} slip and of the accommodation mechanism are not shown in Fig. 4 since they are small (always less than 10%). It can be observed that the contribution of [100] globally increases with time, i.e. as the polycrystal reaches shallower depths. [001] and [100] exhibit similar activities before the flow corner although [001](010) is by far the softest system. Slip on [100] becomes dominant at shallower depths.

The associated LPO development is shown in Fig. 5 at three different times, i.e. just before the flow corner (overall strain ∼0.52) where the polycrystal has experienced essentially vertical simple shear, just after the flow corner (strain ∼1.05) during which the polycrystal is submitted to significant axial straining, and at the end of the streamline (strain ∼2.1) where deformation consists essentially of a horizontal simple shear. The overall tendency is an alignment of the [100] axes with the long axis of the finite strain ellipsoid with an anticlockwise rotation of a axes after the flow corner, a feature that has been also observed in [59] for conditions for which [100] was by far the most active slip direction. However, LPOs remain rather smooth along the upwelling path, and strengthen significantly only at the flow corner. It can also be noticed that, owing to the rotation component of the prescribed velocity gradient and to the rapid change of the deformation path, less pronounced textures are obtained at the end of the streamline than at the flow corner, although olivine is subjected to larger strain. Obviously, the sharp predicted LPOs associated with the small number of available slip system are likely to be at the origin of a very strong viscoplastic anisotropy at the polycrystal scale, as in [59].

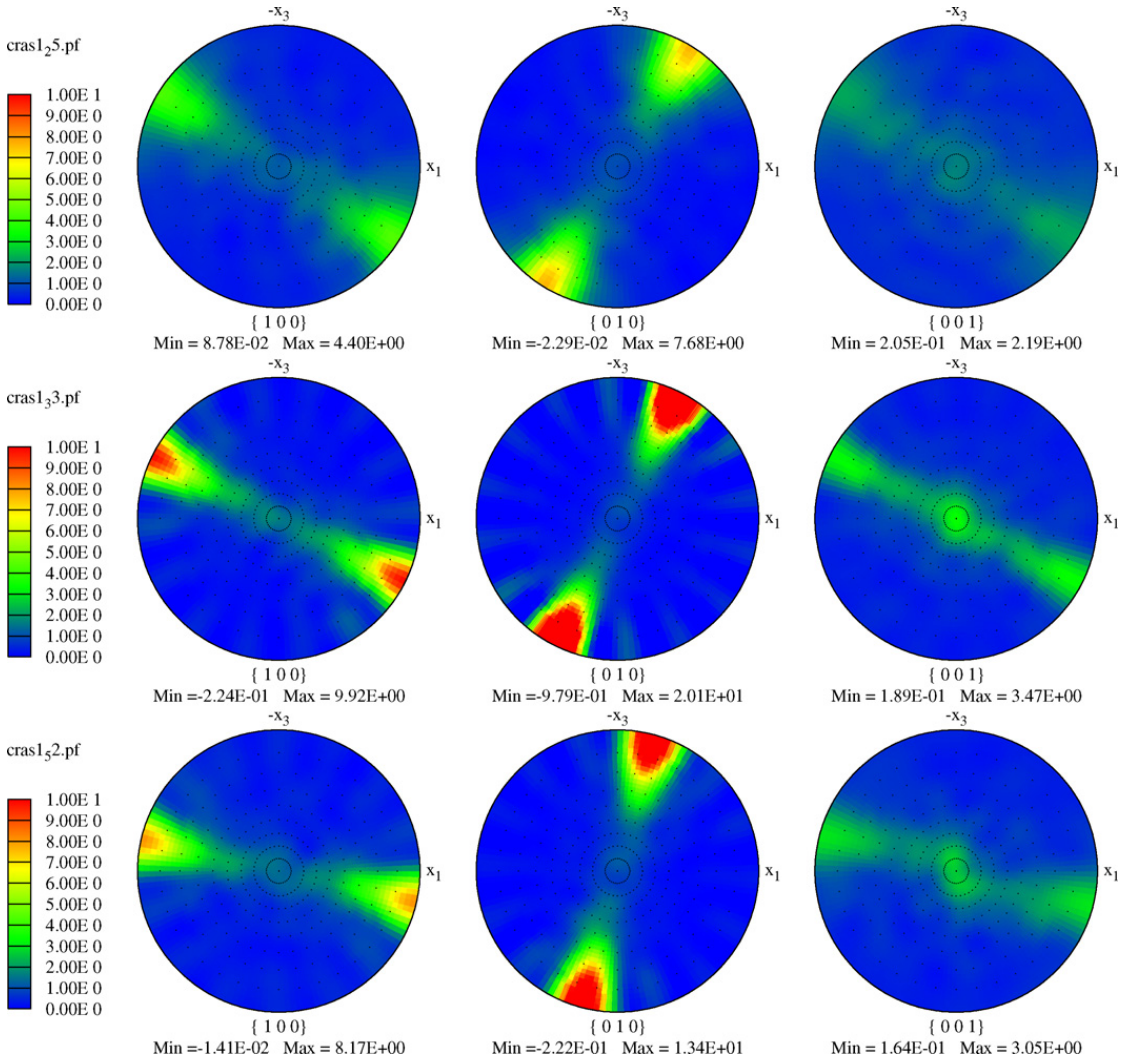

Fig. 5. Pole figures of olivine polycrystals predicted by the SO self-consistent scheme along streamline $\psi_0 = 1200$ m^2/a after (top) 25 Ma corresponding to an equivalent strain of 0.52 and in situ depth of 140 km, (center) 33 Ma (strain = 1.05, depth = 92 km), and (bottom) 52 Ma (strain = 2.1, depth = 67 km). Initial polycrystal at 410 km depth was randomly oriented (pole figure intensities equal to 1). Stereographic projections plotted in the macroscopic ($\mathbf{x}$, $\mathbf{z}$) axes defined in Fig. 3a.

Fig. 5. Figures de pole de polycristaux d'olivine prédites par l'extension SO du schéma auto-cohérent, le long de la ligne de courant $\psi_0 = 1200$ m^2/a et à (haut) 25 Ma, ce qui correspond à une déformation équivalente de 0,52 et une profondeur de 140 km, (milieu) 33 Ma (déformation = 1,05, profondeur = 92 km), et (bas) 52 Ma (déformation = 2,1, profondeur = 67 km). Projections stéréographiques tracées dans les axes macroscopiques ($\mathbf{x}$, $\mathbf{z}$) définis sur la Fig. 3a.

The above results suggest the following comments:

- Additional numerical tests for which the CRSS of all slip systems have been kept constant along the streamline show that although rather sharp LPOs are obtained, LPO evolution has only a modest influence on slip system activities for most systems. Only the activity of [100](010) needs to be increased significantly at 30 Ma for the flow to turn the corner, due to the LPO-induced anisotropy. Consequently, evolutions of slip system activities in Fig. 4 are likely to result essentially from LPO development. The effect of CRSS evolution with P–T (i.e. depth) is surprisingly small; it seems to express itself essentially in the decreasing activity of [001](010) and in increasing activity of [100]{021}, corresponding to the respective hardening and softening of those systems.
- For simpler deformation paths such as simple shear, it can be shown that whatever the CRSS considered (i.e. corresponding to either high or low P–T conditions), the overall tendency found with the SO model is an alignment of (010) plane with the shear plane and an alignment of [100] direction with the shear direction. This corresponds to the so-called *Type-A* texture according the classification of [60]. It is worth noting that such LPOs are also obtained with dominant slip on [001](010) (e.g. for CRSS corresponding to high P) as far the total slip on [100] is slightly larger than that on [001], although the literature attributes Type-A textures to dominant [100](010) slip. This is also the case obtained here (Fig. 4).
- The intensity of (010) pole figures predicted by our multiscale approach is found to be systematically larger than that for (100) or (001) pole figures. To the best of our knowledge, this tendency has not been reported on experimental

studies of olivine deformation. Precise LPO analysis on experimentally deformed aggregates could be used as additional constraints for slip system strength.

- It can be easily shown that Schmid tensors for [100](010), [001](010), and [001](100) are independent with each other (a Schmid tensor $\boldsymbol{\mu}^{(k)}$ relates the RSS on slip system (k) with the local stress $\boldsymbol{\sigma}$ by relation $\tau^{(k)} = \mu_{ij}^{(k)}\sigma_{ij}$). On the other hand, the Schmid tensor for [100](001) is identical to that for [001](100), and those for [100]{021} and [001]{110} are a linear combination of those for [100](010), [001](010), and [001](100). Consequently, slip-rates on [100](001), [100]{021} and [001]{110} can be directly deduced from those on [100](010), [001](010), and [001](100).
- There are however other features in those results that are far not intuitive, as for instance the link between the CRSS of a system and its activity. It is generally admitted that the activity of a hard system is smaller that than of a soft system. This is certainly the case for materials with relatively small plastic anisotropy at the grain scale. Olivine, however, exhibits a huge anisotropy owing to the lack of independent slip systems. Our numerical tests show that hard slip systems often exhibit a larger activity than soft systems. For example in Fig. 4, the activity of [001](010) at 52 Ma (recall that activities are almost LPO independent) is larger than all other systems although it is one of the hardest systems (CRSS of 2.29 compared to 1 for [100](010) and 1.21 for [100]{021}, [001](100), and [100](001)).
- The case of system [001]{110} is also worth discussing. As stated earlier, its CRSS has been set to three times that for [001](100) although considerations on dislocation structure would rather indicate a similar CRSS for both. It turns out that if the CRSS of [001]{110} is indeed taken equal to that of [001](100), final LPOs at shallow depth exhibit a marked Type-B component (i.e. with [001] axes subparallel to the shear direction). Such crystallographic textures are not realistic for low P conditions, and therefore we were forced to strengthen [001]{110} to decrease its activity. This shows that this system, which rheology has not been clearly characterized both experimentally and theoretically (see discussion in Section 2), and which is not expected to be a dominant slip system, seems to have a great influence on in situ LPOs.

4. Concluding remarks

The aim of this work was to couple leading-edge experimental, theoretical, and numerical techniques to get an improved understanding of olivine rheology and potential microstructures developing in the Earth's upper mantle. This provides, to the best of our knowledge, the very first multiscale approach applied to mantle dynamics, covering scales ranging from the dislocation-core structure (nm) to that of the Earth's mantle (km or larger scale). Pressure and temperature dependent strength of olivine slip systems at the grain scale are estimated with state-of-the-art deformation experiments using a D-DIA apparatus installed on synchrotron facilities. Those data are enriched by first-principle calculations for dislocation-core structures and lattice friction. Depth dependent slip system strengths are finally introduced in a mean-field micromechanical model that has been validated on reference full-field numerical results obtained on olivine aggregates. We stress that the use of mean-field micromechanical models that capture accurately the mechanical interaction between the deforming grains, such as the second-order self-consistent scheme of Ponte Castañeda [10], is a requisite condition to make the correct link between processes at the slip system level and the overall polycrystal response. There are many features arising in the plasticity of highly anisotropic polycrystals such as olivine that are far from being intuitive, as discussed above, and most of them are not captured by ad hoc or simple micromechanical models.

There are evidently many aspects that have been left besides in this work for a proper application to the Earth's mantle, such as (i) the effect of extremely small in situ strain-rate, about 10 orders of magnitude smaller than standard strain-rates used during laboratory experiments, (ii) the effect of recrystallization on LPO, that is only poorly understood at present, (iii) the feedback that LPO-associated anisotropy might have on in situ flow – and thus on LPO development, (iv) the effect of other mineral phases present in the upper mantle such as pyroxenes which slip system anisotropy is even larger than for olivine, etc. Some of these aspects will be investigated in forthcoming work.

Acknowledgements

This research was supported by the Centre National de la Recherche Scientifique CNRS/INSU Grants "DyETI 2005", the CNRS "Programme International de Collaboration Scientifique" (PICS program), as well as the Agence Nationale de la Recherche (ANR) Grant BLAN08-2_343541 "Mantle Rheology". O. Castelnau wishes to thank D.K. Blackman for the many discussions on mantle dynamic.

References

[1] T.W. Becker, S. Chevrot, V. Schulte-Pelkum, D.K. Blackman, Statistical properties of seismic anisotropy predicted by upper mantle geodynamic models, J. Geophys. Res. 111 (2006) B08309, doi:10.1029/2005JB004095.
[2] D.K. Blackman, Use of mineral physics, with geodynamic modeling and seismology, to investigate flow in the Earth's mantle, Rep. Prog. Phys. 70 (2007) 659–689.
[3] P. Raterron, S. Merkel, In situ rheological measurements at extreme pressure and temperature using synchrotron X-ray diffraction and radiography, J. Synchr. Rad. 16 (2009) 748–756.
[4] J. Durinck, A. Legris, P. Cordier, Pressure sensitivity of olivine slip systems: first-principle calculations of generalized stacking faults, Phys. Chem. Miner. 32 (2005) 646–654.

[5] J. Durinck, P. Carrez, P. Cordier, Application of the Peierls–Nabarro model to dislocations in forsterite, Eur. J. Mineral. 19 (2007) 631–639.
[6] J. Durinck, B. Devincre, L. Kubin, P. Cordier, Modeling the plastic deformation of olivine by dislocation dynamics simulations, Am. Mineral. 92 (2007) 1346–1357.
[7] P. Carrez, A.M. Walker, A. Metsue, P. Cordier, Evidence from numerical modelling for 3D spreading of [001] screw dislocations in Mg_2SiO_4 forsterite, Philos. Mag. 88 (2008) 2477–2485.
[8] H.R. Wenk, C.N. Tomé, Modelling dynamic recrystallization of olivine aggregates deformed in simple shear, J. Geophys. Res. 104 (1999) 25513–25527.
[9] A. Tommasi, D. Mainprice, G. Canova, Y. Chastel, Viscoplastic self-consistent and equilibrium-based modeling of olivine lattice preferred orientations: implications for the upper mantle seismic anisotropy, J. Geophys. Res. 105 (2000) 7893–7908.
[10] P. Ponte Castañeda, Second-order homogenization estimates for nonlinear composites incorporating field fluctuations. I – Theory, J. Mech. Phys. Solids 50 (2002) 737–757.
[11] M.I. Idiart, H. Moulinec, P. Ponte Castañeda, P. Suquet, Macroscopic behavior and field fluctuations in viscoplastic composites: Second-order estimates versus full-field simulations, J. Mech. Phys. Solids 54 (2006) 1029–1063.
[12] R.A. Lebensohn, C.N. Tomé, P. Ponte Castañeda, Self-consistent modeling of the mechanical behavior of viscoplastic polycrystals incorporating field fluctuations, Philos. Mag. 87 (28) (2007) 4287–4322.
[13] O. Castelnau, D.K. Blackman, R.A. Lebensohn, P. Ponte Castañeda, Micromechanical modelling of the viscoplastic behavior of olivine, J. Geophys. Res. 113 (2008) B09202, doi:10.1029/2007JB005444.
[14] O. Castelnau, R.A. Lebensohn, P. Ponte Castañeda, D.K. Blackman, Earth mantle rheology inferred from homogenization theories, in: O. Cazacu (Ed.), Multi-Scale Modeling of Heterogeneous Materials, Wiley, ISBN 9781848210479, 2008.
[15] H. Couvy, D.J. Frost, F. Heidelbach, K. Nyilas, T. Ungar, S. Mackwell, P. Cordier, Shear deformation experiments of forsterite at 11 GPa–1400 °C in the multianvil apparatus, Eur. J. Mineral. 16 (2004) 877–889.
[16] D. Mainprice, A. Tommasi, H. Couvy, P. Cordier, D.J. Frost, Pressure sensitivity of olivine slip systems and seismic anisotropy of Earth's upper mantle, Nature 433 (2005) 731–733.
[17] P. Raterron, J. Chen, L. Li, D. Weidner, P. Cordier, Pressure-induced slip-system transition in forsterite: single-crystal rheological properties at mantle pressure and temperature, Am. Mineral. 92 (2007) 1436–1445.
[18] H. Jung, W. Mo, H. Green, Upper mantle seismic anisotropy resulting from pressure-induced slip transition in olivine, Nat. Geosci. 2 (2009) 73–77.
[19] P. Raterron, E. Amiguet, J. Chen, L. Li, P. Cordier, Experimental deformation of olivine single crystals at mantle pressures and temperatures, Phys. Earth Planet. Interiors 172 (2009) 74–83.
[20] Z. Xu, Q. Wang, S. Ji, J. Chen, L. Zeng, J. Yang, F. Chen, F. Liang, H. Wenk, Petrofabrics and seismic properties of garnet peridotite from UHP Sulu terrane (China): Implications for olivine deformation mechanism in a cold and dry subducting continental slab, Tectonophysics 421 (2006) 111–127.
[21] S. Ji, Q. Wang, Z. Xu, Reply to the comment of S. Karato on "Petrofabrics and seismic properties of garnet peridotites from the USP Sulu Terrane (China)" by Xu et al. [Tectonophysics 421 (2006) 111–127], Tectonophysics 429 (2007) 291–296.
[22] S.I. Karato, Comments on "Petrofabrics and seismic properties of garnet peridotites from the USP Sulu Terrane (China)" by Xu et al. [Tectonophysics 421 (2006) 111–127], Tectonophysics 429 (2007) 287–289.
[23] Q. Bai, S.J. Mackwell, D.L. Kohlstedt, High-temperature creep of olivine single crystals; 1. Mechanical results for buffered samples, J. Geophys. Res. 96 (1991) 2441–2463.
[24] J. Girard, J. Chen, P. Raterron, C. Holyoke, Deformation of single crystal sample using D-DIA apparatus coupled with synchrotron X-rays: In situ stress and strain measurements at high pressure and temperature, J. Phys. Chem. Solids 71 (8) (August 2010) 1053–1058, doi:10.1016/j.jpcs.2010.03.005.
[25] A.M. Walker, B. Slater, J.D. Gale, K. Wright, Predicting the structure of screw dislocations in nanoporous materials, Nat. Mater. 3 (2004) 715–720.
[26] A.M. Walker, J.D. Gale, B. Slater, K. Wright, Atomic scale modelling of the cores of dislocations in complex materials, part 1: methodology, Phys. Chem. Chem. Phys. 7 (2005) 3227–3234.
[27] A.M. Walker, J.D. Gale, B. Slater, K. Wright, Atomic scale modelling of the cores of dislocations in complex materials, part 2: applications, Phys. Chem. Chem. Phys. 7 (2005) 3235–3242.
[28] A.M. Walker, Simulation of screw dislocations in wadsleyite, Phys. Chem. Miner. 37 (5) (2010) 301–310, doi:10.1007/s00269-009-0334-y.
[29] R.E. Peierls, On the size of a dislocation, Proc. R. Soc. Lond. 52 (1940) 34–37.
[30] F.R.N. Nabarro, Dislocations in a simple cubic lattice, Proc. R. Soc. Lond. 59 (1947) 256–272.
[31] V. Vítek, Intrinsic stacking faults in body-centred cubic crystals, Philos. Mag. 18 (1968) 773–786.
[32] J.W. Christian, V. Vítek, Dislocations and stacking faults, Rep. Prog. Phys. 33 (1970) 307–411.
[33] A. Metsue, Modélisation des structures de cœurs des dislocations dans les minéraux du manteau terrestre à l'aide du modèle de Peierls–Nabarro, Ph.D. thesis, Université Lille 1, Lille, France, 2010.
[34] A. Metsue, P. Carrez, C. Denoual, P. Cordier, Plastic deformation of wadsleyite: IV. Dislocation core modelling based on the Peierls–Nabarro–Galerkin model, Acta Mater. 58 (2010) 1467–1478.
[35] Y.B. Chastel, P.R. Dawson, H.-R. Wenk, K. Bennett, Anisotropic convection with implications for the upper mantle, J. Geophys. Res. 98 (1993) 17757–17772.
[36] J.W. Hutchinson, Creep and plasticity of hexagonal polycrystals as related to single crystal slip, Met. Trans. A 8 (9) (1977) 1465–1469.
[37] M.V. Nebozhyn, P. Gilormini, P. Ponte Castañeda, Variational self-consistent estimates for viscoplastic polycrystals with highly anisotropic grains, C. R. Acad. Sci. Paris, Ser. IIB 328 (2000) 11–17.
[38] M.V. Nebozhyn, P. Gilormini, P. Ponte Castañeda, Variational self-consistent estimates for cubic viscoplastic polycrystals: the effects of grain anisotropy and shape, J. Mech. Phys. Solids 49 (2001) 313–340.
[39] R.A. Lebensohn, P. Ponte Castañeda, R. Brenner, O. Castelnau, Full-field vs. homogenization methods to predict microstructure–property relations for polycrystalline materials, in: S. Ghosh, D. Dimiduk (Eds.), Computational Methods for Microstructure–Property Relationships, 2010.
[40] P. Gilormini, Insuffisance de l'extension classique du modèle autocohérent au comportement non linéaire, C. R. Acad. Sci. Paris, Ser. IIB 320 (1995) 115–122.
[41] H. Moulinec, P. Suquet, A numerical method for computing the overall response of nonlinear composites with complex microstructure, Comput. Methods Appl. Mech. Eng. 157 (1998) 69–94.
[42] J.-C. Michel, H. Moulinec, P. Suquet, A computational method based on augmented Lagrangians and Fast Fourier Transforms for composites with high contrast, Comput. Modelling Eng. Sci. 1 (2000) 79–88.
[43] R.A. Lebensohn, N-site modeling of a 3D viscoplastic polycrystal using Fast Fourier Transform, Acta Mater. 49 (2001) 2723–2737.
[44] R.A. Lebensohn, C.S. Hartley, C.N. Tomé, O. Castelnau, Modelling the mechanical response of polycrystals deforming by climb and glide, Philos. Mag. 90 (5) (2010) 567–583.
[45] E. Kröner, Self-consistent scheme and graded disorder in polycrystal elasticity, J. Phys. F: Metal Phys. 8 (1978) 2261–2267.
[46] J.R. Willis, Variational and related methods for the overall properties of composites, Adv. Appl. Mech. 21 (1981) 2–78.
[47] R.A. Lebensohn, O. Castelnau, R. Brenner, P. Gilormini, Study of the antiplane deformation of linear 2-D polycrystals with different microstructure, Int. J. Solids Struct. 42 (2005) 5441–5459.
[48] R. Brenner, R. Lebensohn, O. Castelnau, Elastic anisotropy and yield surface estimates, Int. J. Solids Struct. 46 (2009) 3018–3026.

[49] G.W. Milton, The coherent potential approximation is a realizable effective medium scheme, Commun. Math. Phys. 99 (1985) 483–503.
[50] J.D. Eshelby, The determination of the elastic field of an ellipsoidal inclusion, and related problems, Proc. R. Soc. Lond. A 241 (1957) 376–396.
[51] P. Ponte Castañeda, P. Suquet, Nonlinear composites, Adv. Appl. Mech. 34 (1998) 171–302.
[52] R. Brenner, O. Castelnau, L. Badea, Mechanical field fluctuations in polycrystals estimated by homogenization techniques, Proc. R. Soc. Lond. A 460 (2052) (2004) 3589–3612.
[53] P. Gilormini, A critical evaluation for various nonlinear extensions of the self-consistent model, in: A. Pineau, A. Zaoui (Eds.), Proc. IUTAM Symp. on Micromechanics of Plasticity and Damage of Multiphase Materials, Sèvres, France, 1995, Kluwer Academic Publishers, Dordrecht, 1996, pp. 67–74.
[54] N.M. Ribe, Y. Yu, A theory for plastic deformation and textural evolution of olivine polycrystals, J. Geophys. Res. B 5 (1991) 8325–8335.
[55] H. Mühlhaus, L. Moresi, M. Cada, Emergent anisotropy and flow alignment in viscous rock, Pure Appl. Geophys. 161 (2004) 2451–2463.
[56] E. Lev, B.H. Hager, Prediction of anisotropy from flow models: A comparison of three methods, Geochem. Geophys. Geosyst. 9 (7) (2008) Q07014, doi:10.1029/2008GC002032.
[57] G.K. Batchelor, An Introduction to Fluid Dynamics, Cambridge Univ. Press, New York, 1967.
[58] D.K. Blackman, J.-M. Kendall, Seismic anisotropy in the upper mantle 2. Predictions for current plate boundary flow models, Geochem. Geophys. Geosyst. 3 (9) (2002) 8602.
[59] O. Castelnau, D.K. Blackman, T.W. Becker, Numerical simulations of texture development and associated rheological anisotropy in regions of complex mantle flow, Geophys. Res. Lett. 36 (2009) L12304, doi:10.1029/2009GL038027.
[60] H. Jung, S. Karato, Water-induced fabric transitions in olivine, Science 293 (2001) 1460–1463.